JOURNAL OF PROPULSION AND POWER
Vol. 30, No. 5, September–October 2014

Three-Dimensional Model for Erosion of a Hall-Effect Thruster Discharge Channel Wall

Aaron M. Schinder,* Mitchell Walker,† and Julian J. Rimoli‡
Georgia Institute of Technology, Atlanta, Georgia 30332

DOI: 10.2514/1.B35098

The erosion of the channel wall in Hall-effect thrusters limits the maximum thruster operating lifetime. Hall-effect thruster channel wall materials are often binary composites of BN and SiO_2. The heterogeneity of the material drives the development of complex surface features and roughness during the erosion process. A three-dimensional model of the atomic sputtering of a heterogeneous material is developed. The model investigates, through a ray-tracing technique and empirical erosion rate models of each phase, the interaction between the plasma and the material microstructure. Simulated surface profiles are compared with experimental data collected from the eroded channel wall of the U.S. Air Force Research Laboratory/University of Michigan P5 Hall-effect thruster. The channel wall is composed of M26, a BN-SiO_2 composite material. Simulated surface features and roughnesses for an ion incidence angle of 30 deg resemble those observed through scanning electron microscopy and optical profilometry of the P5 channel wall. Predicted root mean square roughnesses, for 30 deg ion incidence, of 8 μm are within 33% of the 6 ± 2.5 μm root mean square measured experimentally. The composition of the channel wall surface is investigated via x-ray photoelectron spectroscopy and is comparable to prior work, but the reduction in the presence of BN with erosion is not adequately captured by this model.

Nomenclature

B_i	=	angle function fitting parameters
E_{th}	=	threshold energy for sputtering, eV
$f_{v_i}(v_i)$	=	distribution function for single velocity component, #/(m/s)
$f_v(\mathbf{v})$	=	distribution function for ion velocity, $\#/(\text{m/s})^3$
gx, gy	=	average slope in x and y
k	=	sputtering rate scaling parameter
k_b	=	Boltzmann's constant, J/K
$\hat{\boldsymbol{n}}$	=	node surface normal vector
T	=	effective ion temperature, K
$v_{\text{center},i}$	=	component of the mean or bulk velocity of the plasma, m/s
Y	=	sputtering yield for a given incidence angle and impact energy, mm^3/C

I. Introduction

HALL-EFFECT thrusters (HETs) are attractive candidates for many space propulsion applications for commercial, U.S. Department of Defense, and civilian spacecraft, an example being satellite station keeping. HETs typically operate at specific impulses of 1300–3000 s at efficiencies of 50% and greater [1]. Recent qualification life testing of the BPT-4000 HET demonstrated operation of the thruster for 10,400 h [2,3]. One of the limits to HET lifetime is the erosion of the discharge channel wall materials by energetic ions. Figure 1 shows a cross-sectional diagram of a typical HET discharge channel, displaying the channel wall, magnet material, and three regions of interest for erosion. In a HET, gas enters the discharge channel through the anode gas distributor. The neutral gas travels through the channel until it reaches the energetic cloud of electrons trapped by the radial magnetic field near the exit plane of the channel. The gas is ionized by the electrons and then accelerates across a narrow potential drop (usually a few millimeters wide) to a high velocity, at which point it is exhausted from the thruster. One function of the ceramic discharge channel wall of the HET is to protect the magnetic circuit from the energetic plasma. Energetic ions downstream of the accelerating potential drop erode the discharge channel wall over the operational life of the thruster, eventually exposing the magnetic circuit to the plasma. The erosion of the exit-end pole pieces of the magnetic circuit alters the magnetic field topology, which changes the performance of the HET. After the ferrous magnet material begins to sputter, the ejection and subsequent redeposition of the metal onto the spacecraft structure can destroy electrical isolation and degrade the performance of other hardware.

To predict the operational life of the HET, erosion models based on atomic sputtering mechanisms are employed. The current state of the art in the prediction of channel wall erosion involves the use of two-dimensional empirically or numerically derived atomic sputtering models, as well as axisymmetric two-dimensional simulations of the plasma, to produce profiles of the discharge channel wall radius as a function of axial position. Software tools such as HPHall and 1dhydro can be used to perform erosion analysis given a material model [2,4,5]. However, these erosion models have three inherent limitations.

The first limitation of present erosion models is that the experimental data from which they are derived are from experiments that are rarely conducted with ion energies less than 250 eV [6]. In the low discharge voltage modes of HET operation, ion energies of 100–300 eV are present. There are sparse data to build or calibrate the material response at lower energies.

The second limitation of present erosion models is that they model the material as a homogeneous isotropic solid [4]. Consequently, these models have no material-driven basis for the formation of surface features and do not model surface roughness [3]. Microstructural surface features are inherently three dimensional (3-D) and cannot be produced with two-dimensional (2-D) models. These models, having no information about the material, cannot reproduce observed variations in surface composition induced by erosion.

The third limitation of present models is that axisymmetric and 2-D models do not capture the inherently 3-D nature of observed surface features, such as the sawtooth erosion ridges observed during prolonged operation of many Hall-effect thrusters. These ridges are

Presented as Paper 2013-4127 at the 49th AIAA/ASME/SAE/ASEE Joint Propulsion Conference, San Jose, CA, 15–17 July 2013; received 24 July 2013; revision received 31 October 2013; accepted for publication 12 December 2013; published online 9 May 2014.

*Graduate Student, Aerospace Engineering, 270 Ferst Drive NW. Member AIAA.

†Associate Professor, Aerospace Engineering, 270 Ferst Drive NW. Associate Fellow AIAA.

‡Assistant Professor, Aerospace Engineering, 270 Ferst Drive NW; julian.rimoli@aerospace.gatech.edu. Member AIAA (Corresponding Author).

shown for the BPT-4000 thruster in Fig. 2 [3]. Two-dimensional models can only be compared with axisymmetric averages of the erosion depth.

To improve on present models and model the interaction of the plasma with the internal structure and surface of a material, a 3-D model of atomic sputtering was created. Empirical data on the eroded channel wall of the U.S. Air Force Research Laboratory/University of Michigan (AFRL/UM) P-5 thruster were collected to understand the materials and erosion, and as an input to the modeling effort.

To develop a better understanding of the physics and important processes of channel wall erosion, the channel wall of the AFRL/UM P5 HET was investigated using scanning electron microscopy (SEM), x-ray photoelectron spectroscopy (XPS) composition measurements, and optical profilometry. The P5 was operated for more than 1500 h at the University of Michigan. It was operated at power levels of 1.6, 3, and 5 kW under a variety of discharge voltages and flow conditions, as described in the thesis work of Haas [7], Gulczinski [8], and Smith [9]. Table 1 presents a summary of the operating conditions.

Haas [7] and Gulczinski [8] measured the plasma number density profiles and ion energy distributions under these operating conditions. At the 1.6 kW run condition analyzed by Haas, xenon ion number densities were given between 2×10^{17} and 6×10^{17} m^{-3}, and at the 3 kW condition, the ion number densities were between 6×10^{17} and 1×10^{18} m^{-3} [7]. Gulczinski also measured numerous ion energy distribution functions (IEDFs) within and around the channel; at the 1.6 kW run condition, the IEDF centers around 250 eV with roughly a 50 eV full width at half-maximum [8]. To simulate conditions relevant to the environment to which the channel wall has been exposed, the experimental data described earlier are used to define the plasma properties in the numerical model described in Sec. II.

The channel wall of the P5 HET is composed of Combat M26-grade BN-SiO_2. Common materials used for HET discharge channel walls are boron nitride and silica composites (e.g., Combat M and M26) because of their superior machinability and ease of forming over pure BN grades such as A and HBC. The composite is not an isotropic material: In grade M26 (60% BN and 40% silica by mass), highly irregular BN grains are on the order of tens of micrometers wide by hundreds of nanometers thick. These grains are interspersed in a silica matrix, which has large domains of relatively pure silica about 20 μm across. Such microstructures are visible in SEM images of the channel wall, as shown in Fig. 3.

Posttest surface profile and composition data were taken and compared with the results of the model. Three regions of interest were investigated, differing by the degree to which the surface was eroded by contact with the plasma. The regions were termed the noneroded, lightly eroded, and highly eroded regions. The highly eroded region is downstream of the accelerating potential drop and shows markedly different characteristics. Surface profiles of the channel wall surface were taken with an Olympus-LEXT 3-D confocal microscope. XPS spectroscopy yielded information about the surface composition in the three regions. Excerpts from these data are compared with the heterogeneous numerical model in Sec. IV.

Table 1 Summary of AFRL/UM P5 operating conditions

Run condition	Discharge voltage, V	Discharge current, A	Total flow rate, sccm
Gulczinski [8]			
Condition 1	300	5.3	64
Condition 2	500	5.3	64
Condition 3	500	10	111
Haas [7]			
Condition 1	300	5.3	63
Condition 2	300	10	63
Smith [9]			
Condition 1	300	5.3	61
Condition 2	300	10.4	114

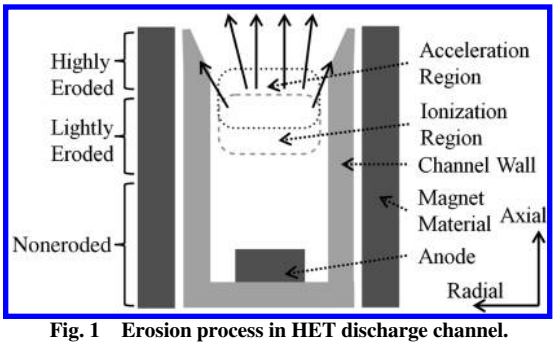

Fig. 1 Erosion process in HET discharge channel.

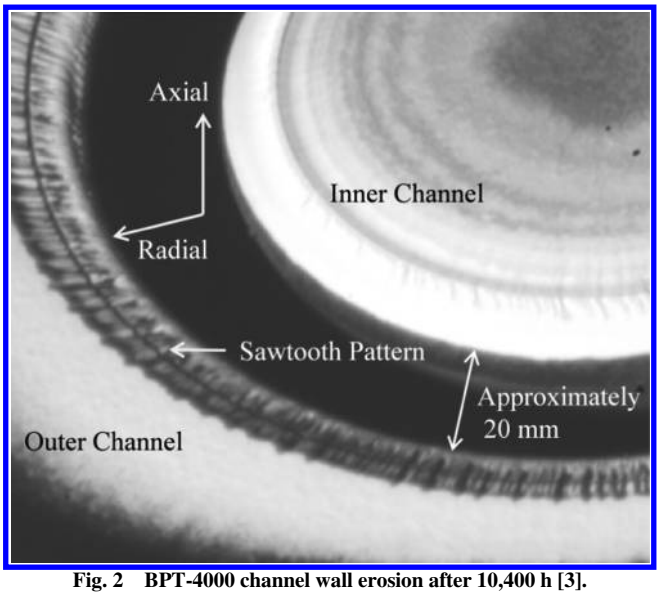

Fig. 2 BPT-4000 channel wall erosion after 10,400 h [3].

II. Model Overview

A. Heterogeneous Model

To simulate the erosion of the channel wall material, a three-dimensional model of the sputtering of a binary material has been developed. This 3-D model reproduces some important features of the surface structures that were found in measurements of the eroded P5 channel wall, and the model provides insight into how a heterogeneous material drives the formation of 3-D surface roughness and geometry. Unlike prior models that generate average behavior, the model developed in this work generates surface profiles from the interaction of a plasma with the material microstructure.

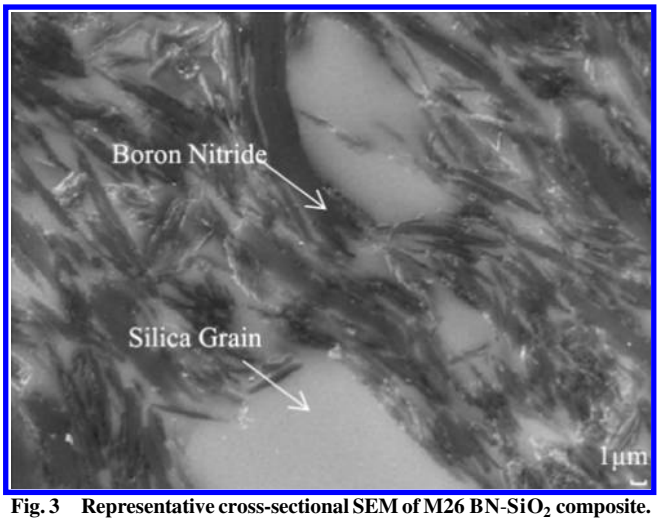

Fig. 3 Representative cross-sectional SEM of M26 BN-SiO_2 composite.

A continuum model of erosion is justified, due to the scale of the atomic sputtering events and the rate at which ion impacts occur. The scale of atomic sputtering events is on the order of 1–10 nm, with yields of cubic nanometers or less per impact, according to the scales of atomic sputtering observed in experiments [6,10,11] and computational tools such as Stopping and Range of Ions in Matter (SRIM 2008). The grid spacing chosen during simulation is on the order of tenths of micrometers for the small-scale domain model, and 1 μm for the large-scale domain model, with the impact rate on the order of 10^9 impacts/$\mu m^2 - s$.

Figure 4 depicts the ray-tracing approach used in the present effort. Ray-tracing techniques are used to determine the regions of the material surface that are exposed to ion bombardment, or that are shadowed. The algorithm for determining geometry and shadowing is described in Secs. II.C and II.D. Each material phase has its own component atomic sputtering model, which returns the sputtering yield as a function of impact angle and energy. Both BN- and SiO_2-exposed surfaces have a separate angle and energy dependence to their yield functions and erosion rates, described in Secs. II.E and II.F. The ion impact angles are calculated based on the local incidence angle of each velocity component of the plasma.

B. Flow of Execution

The sputtering model consists of a model of the 3-D material domain, a model of either an ion beam or a distribution of velocities in a plasma with an ion energy distribution, and a model of the two-dimensional surface geometry. During the modeling of erosion, a volumetric region of material information is generated, and the surface mesh is initialized at the top of the simulation domain. For each time step, the material type at each point on the surface is calculated, along with the local surface normal vectors. Then, the shadowing is calculated to determine whether or not ions can impact each point on the surface. Next, the local erosion rate is calculated as a function of the material, the ion energy and direction, and the local surface normal. Finally, the surface mesh geometry is updated. Figure 5 shows the sequence of execution for the model.

C. Discretization Scheme

The surface is discretized as a two-dimensional regular grid. For each point on the surface, the local normal is calculated in terms of the height of the four adjacent nodes. The local surface area exposed for each node is the cell area divided by the cosine of the local surface normal angle with the vertical. Figure 6 shows a projection of the relative nodes used in calculating shadowing and the local surface normal.

The local surface normals are calculated as shown in Eq. (1), where g_x and g_y are placeholder variables for components of the normal vector $\hat{\boldsymbol{n}}$; x, y, $z_{i,j}$ are the coordinates of the current node; and the increments of the subscript (i, j) refer to the positions of the neighboring nodes:

$$\begin{cases} g_x = \frac{1}{2}\left(\frac{z_{i+1,j}-z_{i,j}}{x_{i+1,j}-x_{i,j}}\right) + \frac{1}{2}\left(\frac{z_{i,j}-z_{i-1,j}}{x_{i,j}-x_{i-1,j}}\right) \\ g_y = \frac{1}{2}\left(\frac{z_{i,j+1}-z_{i,j}}{y_{i,j+1}-y_{i,j}}\right) + \frac{1}{2}\left(\frac{z_{i,j}-z_{i,j-1}}{y_{i,j}-y_{i,j-1}}\right) \\ \hat{\boldsymbol{n}} = \frac{[-gx \quad -gy \quad 1]}{\sqrt{gx^2+gy^2+1}} \end{cases} \tag{1}$$

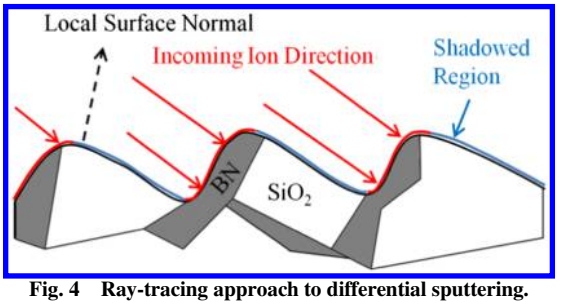

Fig. 4 Ray-tracing approach to differential sputtering.

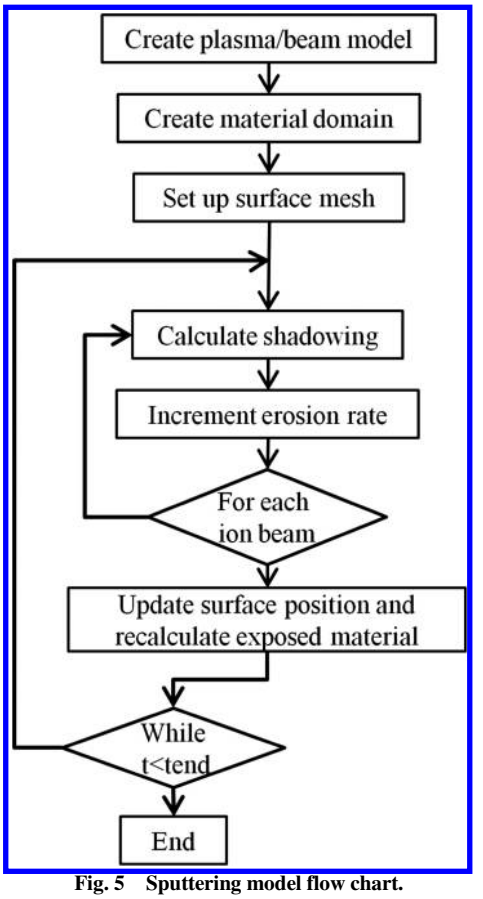

Fig. 5 Sputtering model flow chart.

During each time step, for each ion beam direction, whether or not a given node is in shadow is calculated based on whether or not the ion beam vector intersects any triangle formed by a trio of the nodes along the line of sight of the ion beam vector. To reduce the required computational time, only those nodes along the line of sight are compared when calculating the shadowing.

D. Plasma Model

HETs accelerate ions to a high velocity in a given direction, but also have a distribution of speeds based on where they were ionized within the accelerating potential drop. The simulation software is capable of modeling either a single monoenergetic ion beam or plasma with a distribution of velocities. A first-order model of the plasma is produced using a Gaussian distribution of ion velocities,

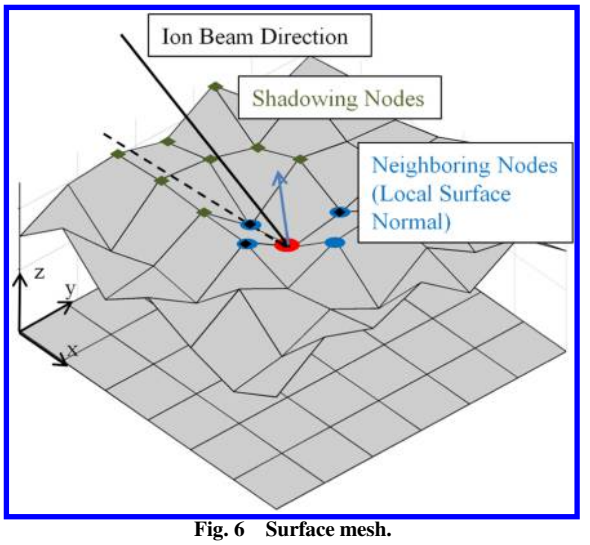

Fig. 6 Surface mesh.

with a pseudotemperature (a measure of the dispersion in ion energies), and an average flow velocity. The single ion beam model is used for moderate incidence angles where the 5 deg of spread in ion angle implied by dispersion in IEDF measurements is not significant. The full plasma model, where the dispersion in ion energies and impact angles is accounted for, is used to model a plasma traveling parallel to the wall, with the variation in normal velocity causing drift into the wall.

The model captures the variation in ion energies and the variation in the angle at which the ions impinge on the surface by dividing a Maxwellian velocity distribution into velocity classes. A center velocity for the plasma is assumed, equal to the mean velocity of the ions after passing across the acceleration potential drop in the discharge channel. An effective pseudotemperature for the ion energy is also assumed, chosen based on the ion energy distribution measurements in the works of Gulczinski [8] and Haas [7], which suggests a Gaussian distribution of velocities around the center velocity. For each dimension of velocity space, the distribution is then partitioned into velocity classes. The fraction of the total ion number density is binned for each of these velocity classes, and this fraction is normalized so that the total fraction for all bins sums to one. An ion beam structure is created for each velocity class, with the energy and direction calculated from the center velocity of the velocity class bin. Equation (2) shows the expression for a Gaussian velocity distribution offset by the center velocity for the equivalent beam; f_{vi} is the normalized distribution function, m is the mass of the ion, k_b is Boltzmann's constant, and v_i is a component of the ion velocity:

$$\begin{cases} f_{v_i}(v_i) = \sqrt{\frac{m}{2\pi k_b T}} \exp\left(\frac{-m}{2k_b T}(v_i - v_{\text{center},i})^2\right) \\ f_v(\mathbf{v}) = \prod f_{v_i}(v_i) \end{cases} \tag{2}$$

Using this model, the simulation calculates shadowing and erosion rates for each ion beam. The erosion rates are summed for a total erosion rate, and the surface depths are then updated.

E. Material Domain Model

Two different material domain geometry models are used to capture features and behavior at different scales. Each model uses a different grain geometry and interprets the remaining material as a matrix. On small scales, long, thin triangular BN grains are embedded in a silica matrix. At larger scales, large regions of pure silica are embedded in BN-rich regions.

A small-scale model, an example of which is shown in Fig. 7, with mesh sizes on the order of tens of micrometers on a side, is intended to capture individual BN grains. The BN grains are modeled as triangular flakes interspersed in a silica matrix. The BN grains have a uniformly distributed randomized width and length scale based on minimum and maximum specified lengths and thicknesses. Lengths and thicknesses are chosen to produce material cross sections similar to those imaged experimentally in the SEM of cross sections of the P-5 channel wall material. The grains are placed with a random orientation within the simulation domain until a 60% BN volume fraction is achieved.

The large-scale model, with mesh sizes on the order of hundreds of micrometers, is intended to capture the larger-scale surface roughness and the large silica grains. An example is shown in Fig. 8. These silica grains, modeled as ellipsoidal regions, are placed randomly throughout the domain until a 40% silica volume fraction is achieved. The interstitial area is assumed to be dominated by BN grains, although no attempt is made to resolve the individual grains.

F. Component Atomic Sputtering Models

A homogenous isotropic sputtering model for M26 BN-SiO_2 is provided by Gamero-Castano and Katz [5], who produced a curve fit to experimental data collected by Garnier et al. [6]. Yalin et al. produced experimental atomic sputtering yield data for HBC boron nitride, an almost pure BN material, and for quartz [10]. Quartz is different in structure than the amorphous silica matrix in the BN-SiO_2 composite. Yalin et al.'s data set is used because it has data for both a

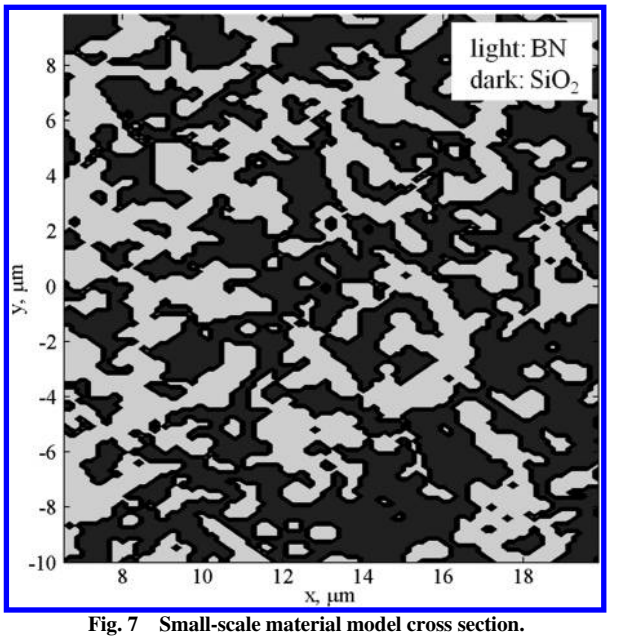

Fig. 7 Small-scale material model cross section.

pure BN and silica material collected via the same method. Curve fits to these data were used for the BN and SiO_2 components of the present model. The models are of a form given in Eq. (3), and the coefficients are listed in Table 2. Y is the sputtering yield in cubic millimeter per Coulomb incident ion current, E is the impact energy in electron volts, E_{th} is the sputtering threshold energy, and α is the incident angle (with respect to the local surface normal) in degrees. The sputtering yield is the volume of material ejected for a given incident current, assumed to be singly ionized, in Coulombs:

$$\begin{aligned} Y(E,\alpha) &= Y_E(E)Y_\alpha(\alpha) \\ &= k(B_0 + B_1\alpha^1 + B_2\alpha^2 + B_3\alpha^3)\sqrt{E}\left(1 - \sqrt{\frac{E_{\text{th}}}{E}}\right)^{2.5} \end{aligned} \tag{3}$$

Figure 9 shows the curve fits to the experimental data at 45 deg ion incidence angle. All data sets have data at this angle. The data provide an example of the large variation in sputtering yield data in the literature. Garnier et al. [6] measured the erosion of M26 with a mass-loss method. Yalin et al. [10] measured sputtering yield by collecting sputtered material on a quartz crystal microbalance, and his data sets

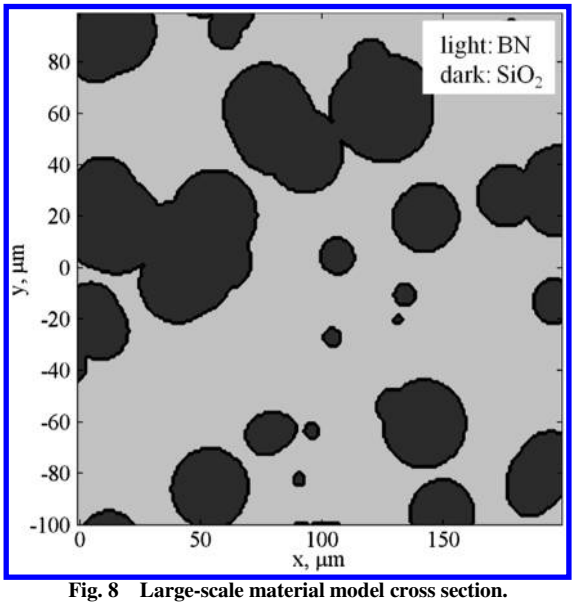

Fig. 8 Large-scale material model cross section.

Table 2 Material model coefficients

Material	Gamero-Castano and Katz [5] M26 (60% BN, 40% SiO_2) [5]	Yalin et al. HBC (99% BN) [10]	Yalin et al. quartz (silica) [10]
E_{th}, eV	58.6	18.3	18.3
B_0	9.90E − 03	1.18	9.14E − 01
B_1	0	1.94E − 02	5.34E − 02
B_2	6.04E − 06	1.22E − 04	−6.98E − 04
B_3	−4.75E − 08	−2.22E − 06	3.33E − 06
K	1.00E + 00	2.28E − 03	3.50E − 03

correct for losing mass as nitrogen gas. At ion energies of more than 250 eV, Garnier et al.'s fit for M26 has a higher modeled sputtering yield than Yalin et al.'s model for silica [10]. This may not be physically realistic because silica is the highest yield component of the BN-SiO_2 composite, and BN-SiO_2 is supposed to be lower yield than pure silica. This demonstrates the variation in models for material sputtering in the current use.

G. Analysis of Simulation Convergence

A convergence study was conducted at both small- and large-scale domain sizes to confirm the numerical stability of the simulation. Numerical instability and divergence of the results were found to occur for large time steps, originating in areas of large curvature. The instabilities took the form of ripples in the surface depth, which propagate from these areas. If the ripples are large enough, they interact significantly with the shadowing, and instability results. This effect is most extreme at shallow incidence angles, and so shallow incidence angles were used as the limiting case for the convergence study. Table 3 shows the run conditions of the convergence study.

For the small-domain study, the average erosion rate came to within 5% of the asymptotic value at a time step of 2 s, and the rms roughness of the produced profiles converged. For the large-domain study, the average erosion rate approached 0.5% of the asymptotic value at a time step of 2 s. Figure 10 shows the convergence of the average erosion rates. These time steps were used in subsequent simulations at these relative mesh sizes.

A brief sensitivity analysis was conducted to test variations in the solutions with variations in the sputtering yield of each component. The conditions of the large-domain study were used, with an ion incidence angle of 30 deg. In the nominal case, model parameters were left as in Table 2, and the rms roughness at 250 μm erosion depth was 5.8 μm. Adjusting the k parameters to the extreme limits of Yalin et al.'s data set (highest yield for SiO_2 lowest for BN) [10], $K_{BN} = 1.87E-3$, $K_{SiO_2} = 4.93E-3$, rms roughness at 250 μm is 11.1 μm. The error bars for component yield overlap, and so the other extreme would yield 0 μm rms roughness. The rms roughness achieved at a given erosion depth was found to be proportional to the difference between the sputtering yield parameters.

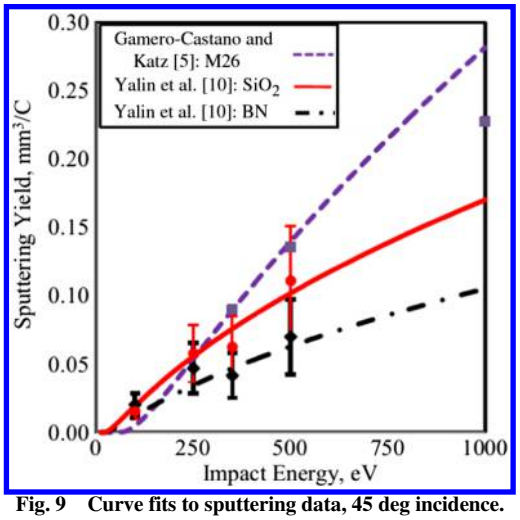

Fig. 9 Curve fits to sputtering data, 45 deg incidence.

Table 3 Convergence study run conditions

	Small-domain study	Large-domain study
Domain size, μm	30 × 16	200 × 100
Mesh	400 × 200	200 × 100
Material	BN Flakes	Ellipsoidal Silica Grains
Minimum length scale, μm	3	0.1
Maximum length scale, μm	10	10
Minimum radius scale, μm	0.1	5
Maximum radius scale, μm	0.4	20
BN volume fraction, %	60	60
Ion energy, eV	245.6	245.6
Incidence angle, deg	1.5	5
No. density, m^{-3}	3E + 17	3E + 17

H. Verification of Implementation

To confirm that the behavior of the model is physically reasonable and obeys the sputtering yield behavior of each component model in the limit of composition, several large-scale material domain models were generated. Each material domain model has a different silica volume fraction, ranging from 0% (no silica grains) to 100% silica. The incidence angle of the ion beam was set at 30 deg. It is expected that the behavior of the model is identical to that of the component models when only that material is present. No surface features should form because the erosion rate is constant across the entire surface.

In addition, the average rate of erosion should be a smooth function of the fraction of the surface composed of each material. The surface features may modify this with the angles with which the ion beams strike the bumps, but it should be a smooth function on average. Figure 11 shows the average erosion rates produced by the models. In the limiting case, where either material fraction is 100%, no surface roughness or features were produced (i.e., the simulation produced a flat surface for each time step) and the recession rate agreed exactly with the component models.

The trend of the series of simulated average erosion rates was bracketed by the component models, and varied smoothly from zero to one. The reproduction of the component model behavior in the limits of composition and well-behaved solutions in between are taken as verification of our implementation of the two-phase model.

One aspect of the behavior of the composition series is that the average erosion rate deviates from a linear relationship between the erosion rates of the two pure-substance models. A linear relationship would be expected of a simple rule of mixture for the exposed material. This extra behavior is an effect of the developing surface structures and highlights the need for models that capture heterogeneous features.

III. Numerical Results

Using the model presented so far, several numerical results were derived. The small-scale material domain model produced profiles similar to the tenth-of-a-micrometer erosion striations seen in close-up SEM imagery of the P5 channel wall surface, as seen in Fig. 12. Ion flow at shallow incidence angles produced long, thin streak lines. Cases where the flow is locally parallel to the larger-scale structure appear to produce these.

The large-scale material domain models provided the most features for comparison with our experimental data from the channel wall. Single ion beam models were used at several angles of attack to the simulated material domain. A thermal distribution of ion beams for a full plasma was used to model a 0 deg incidence case, and 30 deg for comparison with the single ion beam case. Table 4 lists the conditions for the large-domain simulations.

It was found that the distribution of the ion beams at center energies and spread similar to those indicated in the Gulczinski thesis, 250 eV run condition [8] did not differ significantly from the single ion beam case at 30 deg. The effect of the ion energy distribution is most pronounced at shallow incidence angles.

The surface profiles of the simulated regions showed the following in terms of erosion rate as a function of angle: The average erosion

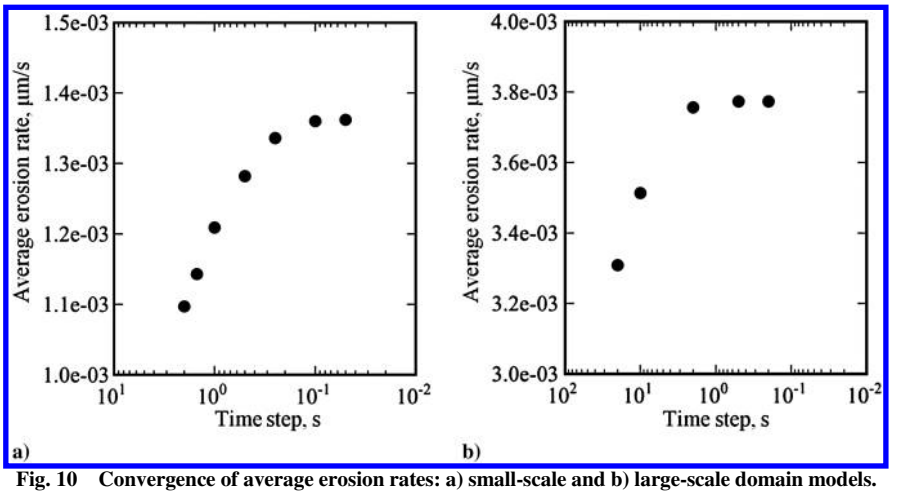

Fig. 10 Convergence of average erosion rates: a) small-scale and b) large-scale domain models.

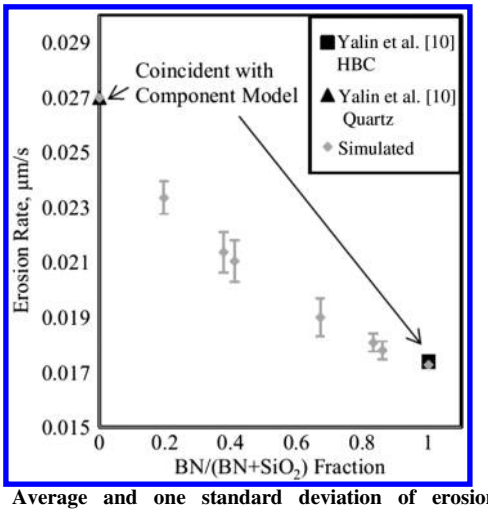

Fig. 11 Average and one standard deviation of erosion rate: comparison with component models.

rate quickly approached a steady-state value, which persisted through the entire evolution of the surface profile, with only minor variations, as shown in Fig. 13.

The surface profiles of the large-scale angle series were not uniform, and developed over time. Eventually, the qualitative nature of the surface appeared to remain unchanged after an erosion depth of ~200 μm. Materials with lower sputtering yields protruded from the surface at various places and eroded away, but the relative magnitude of the features appears stable. The rms roughness of the surface continued to increase throughout the simulated time span, albeit with an apparent logarithmic or asymptotic slowdown as time advanced, corresponding to the mature surfaces. The magnitude of the rms roughness profile that developed, along with the nature of the surface features, is a strong function of the incidence angle of the ion beams.

For example, each of the angle series simulations was run for 18,000 s of simulated time. The 5 deg case achieved a shallower depth at the end of the simulated period. Figure 14 shows the rms roughness achieved at three ion beam incidence angles as a function of erosion depth.

A 24,000 s simulation with a coarser grid and larger domain was run at 30 deg incidence to investigate the boundedness of rms roughness for long erosion times, shown in Fig. 15. At 470 μm erosion depth, the rms roughness was still below 9 μm and was comparable in magnitude to the results from the finer large-scale simulation (Fig. 14). The peak-to-valley roughness did not reach a limit at 470 μm, pointing to the development of larger-scale structures as the simulation advances.

The relative presence of BN relative to SiO_2 is quantified in terms of the proportion of upward-facing area on the simulated domain as a function of time. This measure is proportional to the return from a line-of-sight sensor, such as an XPS, and is insensitive to the area of features like spikes or other projections. The evolution of the BN/SiO_2 ratio is shown in Fig. 16. The ratio appears to increase from 60 to around 70% of the exposed area. The surface BN/SiO_2 ratio remained within 10% of the starting value, the average volume fraction in the material, with no coherent trend up or down as the material erodes. Further variation in the BN/SiO_2 ratio are believed to be due to the size of the material domain. Any local periodic

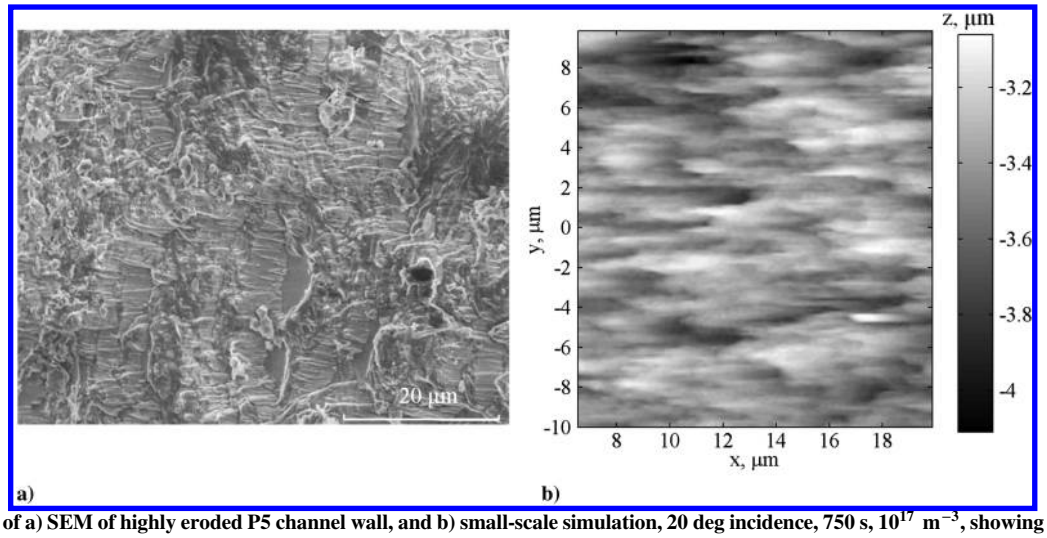

Fig. 12 Images of a) SEM of highly eroded P5 channel wall, and b) small-scale simulation, 20 deg incidence, 750 s, 10^{17} m^{-3}, showing similar patterns.

Table 4 Run conditions, large-scale simulations

Property	Value
Domain	400×200 μm
Mesh	400×200
Material	Ellipsoidal silica grains
Minimum length	0.1 μm
Maximum length	10 μm
Minimum radius	5 μm
Maximum radius	20 μm
BN volume	0.6
Ion beam properties	
Ion energy	250 eV
Angles	[5, 10, 15, 20, 30, 45, 90 deg]
No. density	3.00E + 17m^{-3}
Plasma properties	
Ion temperature	8,000 K
Ion center velocity	19,000 m/s
Angles	0, 30 deg
No. Density	6E + 17 m^{-3}

variation due to eroding through BN grains should be averaged out for large enough surfaces due to their random placement.

IV. Discussion

The first main observation from the model behavior is about the qualitative nature of the generated surface features. Figure 15 shows that the model produced surfaces that were qualitatively mature after erosion depths were achieved on the order of a few times the length of the largest grain features. Local variations in mesh height and feature size appeared to approach a steady state, as did the rms surface roughness. Peak-to-valley roughness, which is sensitive to the largest surface features generated, continued to increase, even after long simulation times and 470 μm erosion depths. This suggests that, with larger domains and longer times, larger-scale surface features may result from the continued operation of the model.

Surface structures observed in SEM imaging of the eroded P5 channel wall were reproduced in the heterogeneous erosion model under certain beam and plasma conditions. The nature of the features produced by the erosion model is highly dependent on the angle at which the ion beam/ion beams impinge on the surface of the material.

SEM imaging of the highly eroded surface showed cliff-and-ridge structures on the order of 20 μm wide and 20–40 μm long. Contrast on the secondary electron emission showed higher BN concentrations near the front of these structures. The large-scale runs also produced similar structures, resulting from the boron nitride shadowing the softer silica grains behind them. The BN ridges shield the silica cliffs from the bulk of the incoming ions. This is shown in Fig. 17. Figure 17 compares an SEM image of the highly eroded region of the P5 with the behavior of the two-phase material model.

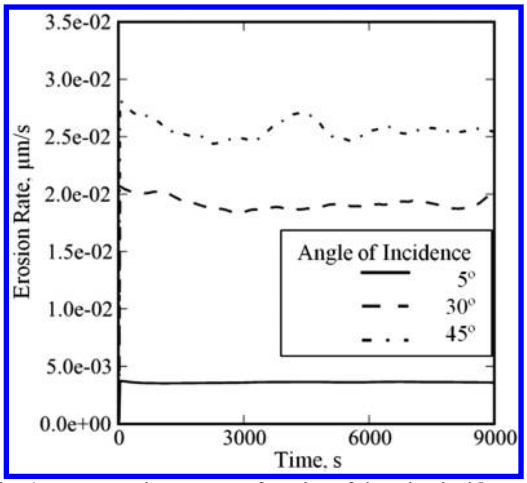

Fig. 13 Average erosion rate as a function of time, ion incidence angles of 5, 30, and 45 deg, large-scale domain model.

For this case, the incidence angle was set to 30 deg, plasma density to 3E17 m^{-3}, and ran for 750 sec.

These cliff-and-valley structures are also comparable in horizontal and vertical magnitude to those seen during profilometry of the eroded channel wall samples. An Olympus LEXT 3-D confocal microscope was used to produce surface profiles of each of the three regions of interest on the samples. In the highly eroded region, the scales of the eroded features in the profiles were similar to those produced by the 30 and 45 deg incidence angle simulations, as shown in Fig. 18. The highlighted region in Fig. 18a is of the same size as the simulated domain in Fig. 18b. Structures of similar size and peak-to-valley depth are developed in the simulation.

The second main observation is the agreement between simulated and empirical rms roughness at a moderate incidence angle. The profilometry of the highly eroded surface indicated an empirical rms roughness of around 6 ± 2.5 μm. This is similar to where the rms roughness of the 30 deg simulated case appeared to asymptote (Figs. 14 and 15). The simulated roughness developed is a function of the largest heterogeneous surface features; in the case of the large-scale material domain model, the 20 μm silica grains govern the erosion.

Not all incidence angles produced surface features and roughnesses comparable to what is seen experimentally. Normal incidence angles produced vertical shapes where the harder to sputter material protruded from the softer silica materials. At parallel incidence angles, the simulated surface was only very slowly eroded, and the aspect ratios of the structures produced tended toward being semi-infinite. This produced a very smooth, polished surface.

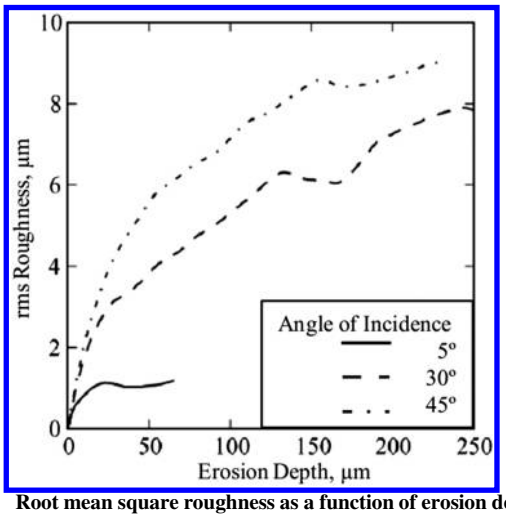

Fig. 14 Root mean square roughness as a function of erosion depth, at ion incidence angles of 5, 30, and 45 deg, large-scale domain model.

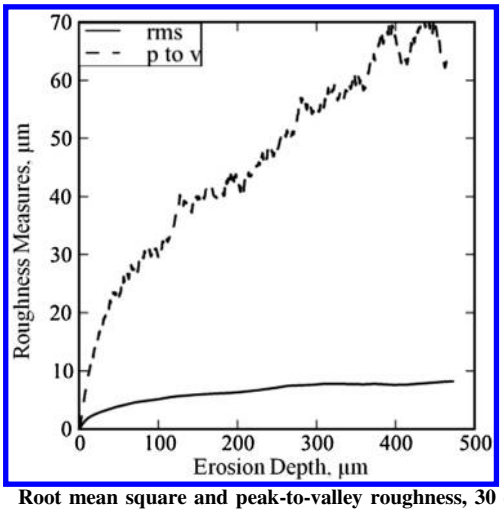

Fig. 15 Root mean square and peak-to-valley roughness, 30 deg ion incidence, large-domain model simulation, with coarse time step, long duration.

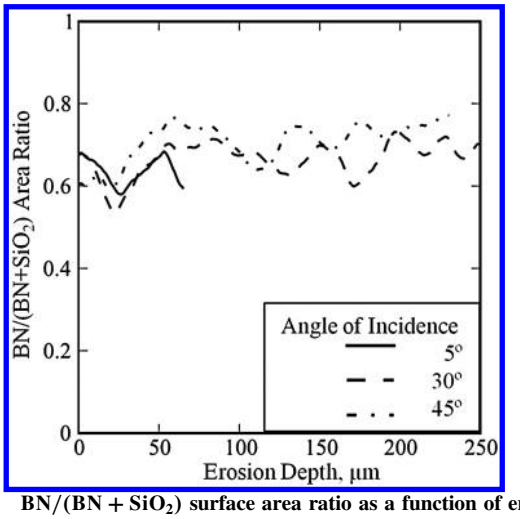

Fig. 16 $BN/(BN + SiO_2)$ surface area ratio as a function of erosion depth, at ion incidence angles of 5, 30, and 45 deg, large-domain simulation.

In the plasma simulation cases when parallel center velocity was assumed, the variation in velocity suggested by Gulczinski's IEDFs produced ion angle distributions with less than 5 deg incidence angle [8]. Simulations including the full plasma model did not produce erosion patterns that were significantly different from cases in which a single ion beam at a shallow incidence angle was used.

Haas's plasma potential contour measurements in the P5 discharge channel suggest that the ions should experience acceleration largely along the axial direction, with little acceleration in the radial direction, as expected of contemporary HET designs [7]. However, note that Haas's measurements were taken at some distance from the wall and do not account for the radial acceleration of ions due to the plasma sheath at the boundary between the channel wall and plasma.

Cross sections of the P5 channel wall have a sharp boundary between the highly eroded and noneroded region shown in Fig. 1, corresponding to the location of the acceleration zone of the plasma. The highly eroded region is inclined to the axis of the channel wall by about 17 deg, suggesting that the plasma was initially impacting the surface at a moderate incidence angle. In summary, the second observation is that we expect to see certain surface features only when ions impact at a given angle.

The third main observation from the model behavior is that surface structures are only generated due to atomic sputtering when there is heterogeneity to the material. In Fig. 11, the pure BN and pure silica models produced flat surfaces that eroded at a rate exactly mirroring that of the pure component sputtering models. In simulated cases, where the erosion was allowed to proceed past the defined material domain into a region of pure material, any surface structure that was produced began to decay back into a flat surface.

The average erosion rate of the surface was between that of the two component atomic sputtering models, as shown in Figs. 11 and 19. However, the variation of the average sputtering rate with mixture fraction was not the linear law of mixtures that was expected from a flat featureless surface. This demonstrates the effect of surface structures on perturbing the average erosion rate. Because of the shadowing effect, the average erosion rate was closer to that of the slower sputtering material than would be expected from a linear law of mixtures.

The fourth main observation concerns the composition of the eroded surface. XPS measurements were taken of the relative concentration of elements on the surface of the eroded channel wall samples. These measurements indicated that BN was depleted relative to silica in the highly eroded region of the thruster. This surprising result mirrors that obtained by Garnier et al. in his erosion experiments on $BN\text{-}SiO_2$ target discs [11]. However, Zidar and Rovey took energy dispersive spectroscopy (EDS) data from an eroded channel wall that instead indicated increased BN presence near the eroded end of the channel wall [12,13], differing from our results and those of Garnier [11]. Figure 20 compares these results. In Fig. 20, XPS Results refers to measurements conducted on the P5 channel wall in the highly eroded and non-eroded region, Garnier's XPS Data refers to measurements taken pre and post-exposure on $BN\text{-}SiO_2$ targets, and Zidar's EDS data refers to EDS taken at 45 and 5 mm from the exit plane of an eroded HET channel wall. Further investigation of the difference between our measurement results would be of interest.

The atomic sputtering model does not account for the observed changes in surface composition. Atomic sputtering alone would predict that BN would protrude from the silica matrix and persist relative to the softer to sputter silica material. The model behavior was such that the relative amount of exposed BN increased slightly but remained within 10% of the average material in the matrix, as shown in Fig. 13.

To illustrate the difficulty with a pure sputtering approach capturing the change in surface composition, a simple analytical model is presented. In the model, a flat surface plane propagates through a regular domain, as shown in Fig. 21. As the surface plane is moved into the domain, the intersection of the surface with the grains produces a similar but translated image to the initial intersection image. According to this model, the exposed area proportion of the BN grains and silica matrix should remain exactly the same. In a sputtering model, this may be modified due to exposure of the lower-yield grains, but significant variation is not observed in the present model of $BN\text{-}SiO_2$.

If the analytical model is modified so that when BN grains, which lose a critical amount of support in the surrounding matrix, are removed, it could account for changes in the silica. In this model, depicted in Fig. 22, the BN grains protrude from the matrix as it is sputtered. When the BN has a small enough supporting surface area in the silica, they are removed, leaving a shallow groove behind. In this case, the upward facing area due to silica increases after BN grains are removed.

To explain the variation in surface composition, another mechanism, such as the grain-ejection mechanism proposed, is needed. Atomic sputtering does not predict the decrease in BN in the highly eroded region. Grain ejection provides a plausible mechanism that could explain this surprising observation.

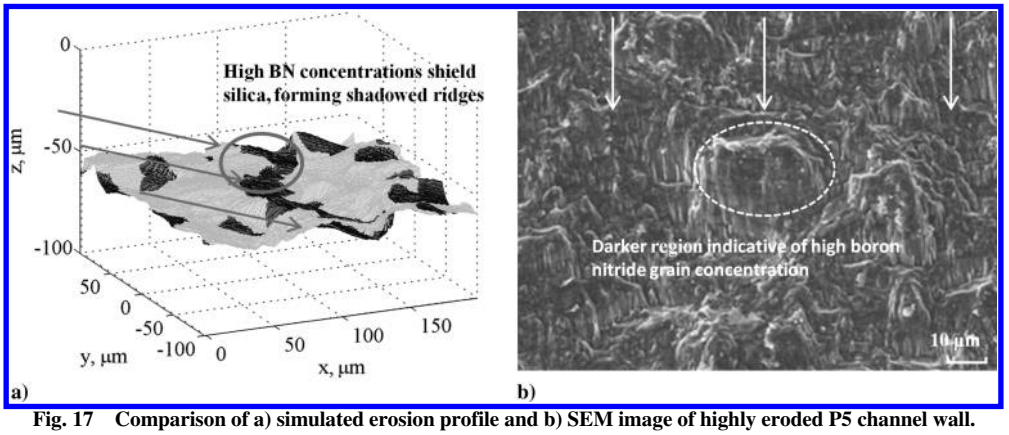

Fig. 17 Comparison of a) simulated erosion profile and b) SEM image of highly eroded P5 channel wall.

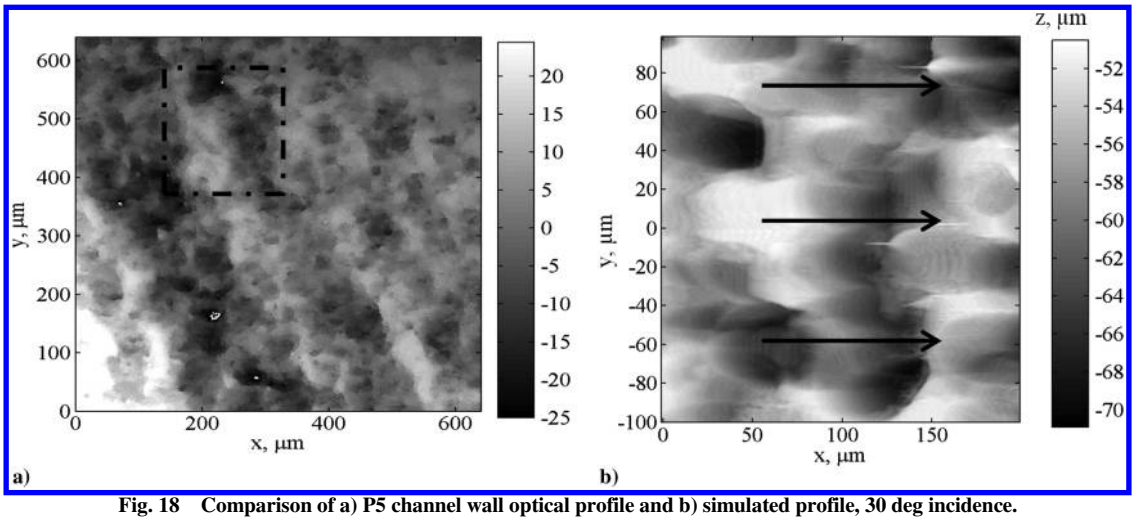

Fig. 18 Comparison of a) P5 channel wall optical profile and b) simulated profile, 30 deg incidence.

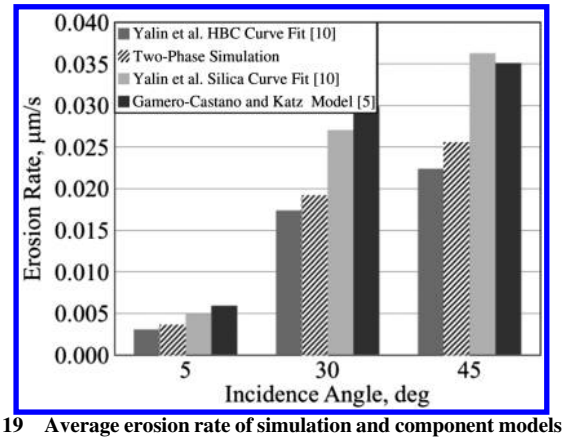

Fig. 19 Average erosion rate of simulation and component models as a function of incidence angle.

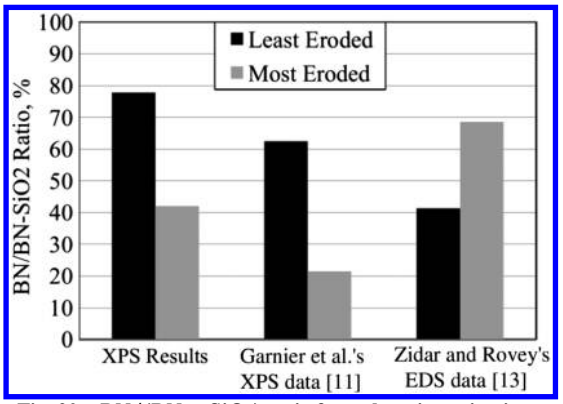

Fig. 20 $BN/(BN + SiO_2)$ ratio from three investigations.

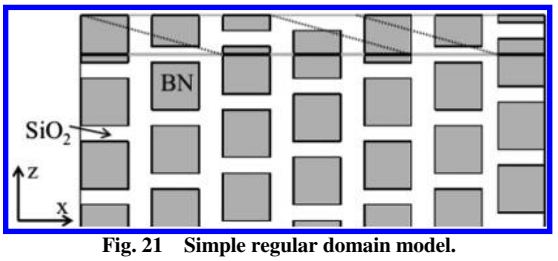

Fig. 21 Simple regular domain model.

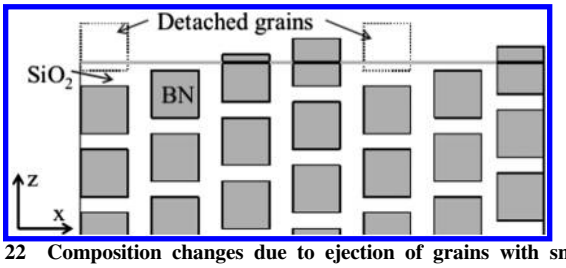

Fig. 22 Composition changes due to ejection of grains with small support.

V. Conclusions

The modeling of atomic sputtering of a heterogeneous material is capable of reproducing some features observed experimentally in an eroded channel wall. The ridge and cliff structure to the surface is explained by BN, which has a lower sputtering rate, shadowing the silica material behind it. The surface features produced by the model are a strong function of the incidence angle of the ions. The observed ridge and cliff structures are similar to those produced by ions, which impact at an angle of 30 deg. Experimental rms roughnesses in the eroded channel wall are similar to those produced by the model for incidence angles of 30 deg. This suggests that the plasma was impacting the P5 channel wall at a moderate angle of incidence. Variation in the modeled material composition produced variations in the average erosion rate, as expected. However, the average erosion rate deviated from what was expected from a simple law of mixtures, which demonstrates the significance of the surface structure and shadowing. Average erosion rates are biased toward those of the component with the lowest sputtering rate in the material mixture. The relative absence of BN in XPS measurements of the surface of a channel wall in the highly eroded region remains unexplained, because this behavior is not captured in a pure atomic sputtering model. Theoretical reason to believe that sputtering cannot explain this behavior was presented. The ejection of BN grains with small support in the matrix is a plausible mechanism by which this surprising experimental variation in composition can be explained.

Acknowledgments

This material is based upon work supported by the U.S. Air Force Office of Scientific Research under grant FA9550-11-1-0160. The authors would like to acknowledge Gregory Thompson and Thomas Burton of the University of Alabama for their scanning electron microscopy and x-ray photoelectron spectroscopy of the P5 channel wall, sample preparation work, and material science expertise.

References

[1] Dudeck, M., Doviel, F., Arcis, N., and Zurbach, S., "Plasma Propulsion for Geostationary Satellites and Interplanetary Spacecraft," *Romanian Journal of Physics*, Vol. 56, 2011, pp. 3–14.

[2] Hofer, R., Mikellides, I., and Katz, I., "BPT-4000 Hall Thruster Discharge Chamber Erosion Model Comparison with Qualification Life Test Data," *30th International Electric Propulsion Conference*, IEPC-2007-267, Florence, Italy, 2007.

[3] De Grys, K., Mathers, A., Welander, B., and Khayms, V., "Demonstration of 10,400 Hours of Operation on a 4.5 kW Qualification Model Hall Thruster," *AIAA Joint Propulsion Conference*, AIAA Paper 2010-6698, 2010.

[4] Yim, J. T., "Computational Modeling of Hall Thruster Channel Wall Erosion," Ph.D. Thesis, Univ. of Michigan, Ann Arbor, MI, 2008.

[5] Gamero-Castano, M., and Katz, I., "Estimation of Hall Thruster Erosion Using HPHall," *29th International Electric Propulsion Conference*, IEPC 2005-303, Jet Propulsion Laboratory, CA, Oct. 2005.

[6] Garnier, Y., Viel, V., Roussel, J. F., and Bernard, J., "Low-Energy Xenon Ion Sputtering of Ceramics Investigated for Stationary Plasma Thrusters," *Journal of Vacuum Science and Technology*, Vol. 17, No. 6, 1999, pp. 3246–3254.
doi:10.1116/1.582050

[7] Haas, J. M., "Low-Perturbation Interrogation of the Internal and Near-Field Plasma Structure of a Hall Thruster Using a High-Speed Probe Positioning System," Ph.D. Thesis, Univ. of Michigan, Ann Arbor, MI, 2001.

[8] Gulczinski, F. S., "Examination of the Structure and Evolution of Ion Energy Properties of a 5 kW Class Laboratory Hall Effect Thruster at Various Operational Conditions," Ph.D. Thesis, Univ. of Michigan, Ann Arbor, MI, 1999.

[9] Smith, T. B., "Deconvolution of Ion Velocity Distributions from Laser-Induced Fluorescence Spectra of Xenon Electrostatic Thruster Plumes," Ph.D. Thesis, Univ. of Michigan, Ann Arbor, MI, 2003.

[10] Yalin, A. P., Rubin, B., Domingue, S. R., Glueckert, Z., and Williams, J. D., "Differential Sputter Yields of Boron Nitride, Quartz, and Kapton Due to Low Energy Xe+ Bombardment," AIAA Paper 2007-5314, July 2007.

[11] Garnier, Y., Viel, V., and Roussel, J., "Investigation of Xenon Ion Sputtering of One Ceramic Material Used in SPT Discharge Chamber," *26th International Electric Propulsion Conference*, IEPC-1999-083, 1999, pp. 512–517.

[12] Zidar, D. G., and Rovey, J. L., "Hall-Effect Thruster Channel Surface Properties Investigation," *Journal of Propulsion and Power*, Vol. 28, No. 2, 2012, pp. 334–343.
doi:10.2514/1.B34312

[13] Zidar, D., and Rovey, L., "Boron Nitride Hall-Effect Thruster Channel Surface Properties Investigation," *AIAA Joint Propulsion Conference*, AIAA Paper 2011-5993, 2011.

J. Blandino
Associate Editor